ACS APPLIED MATERIALS & INTERFACES

Research Article

www.acsami.org

Graphene-Diatom Silica Aerogels for Efficient Removal of Mercury Ions from Water

Shervin Kabiri, Diana N. H. Tran, Sara Azari, and Dusan Losic*

School of Chemical Engineering, The University of Adelaide, Adelaide, SA 5005, Australia

Supporting Information

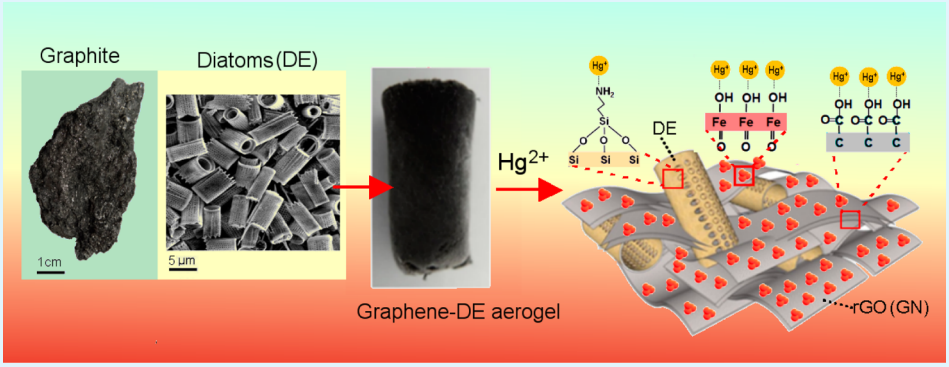

ABSTRACT: A simple synthetic approach for the preparation of graphene-diatom silica composites in the form of self-assembled aerogels with three-dimensional networks from natural graphite and diatomite rocks is demonstrated for the first time. Their adsorption performance for the removal of mercury from water was studied as a function of contact time, solution pH, and mercury concentration to optimize the reaction conditions. The adsorption isotherm of mercury fitted well with the Langmuir model, representing a very high adsorption capacity of >500 mg of mercury/g of adsorbent. The prepared aerogels exhibited outstanding adsorption performance for the removal of mercury from water, which is significant for environmental applications.

KEYWORDS: *graphene, diatomaceous earth, aerogel, adsorption, mercury*

1. INTRODUCTION

Heavy metals have been excessively released into the environment due to rapid industrialization that has created serious global concerns. Mercury, in particular, is recognized as one of the most harmful pollutants in the environment because of its high toxicity, volatility, and bioaccumulation, which is often introduced to the environment through industrial wastewaters, electroplating and metal finishing, mining activities, fertilizers, and pharmaceuticals.[1,2] The disposed mercury (both inorganic and organic forms) can be accumulated in the human body, causing adverse effects by impairing mental and neurological functions.[3,4] Therefore, preventing contamination and efficiently removing mercury from the environment is recognized as one of the top priorities by the World Health Organization (WHO).[4]

Adsorption methods emerged as the most promising technologies for mercury removal from waters where numerous synthetic and natural porous materials have been explored and commercially used.[5−7] Thus far, activated carbons and synthetic silica mesoporous materials (MCM-41 and SBA-15) are the most successful adsorbents on the market. However, these adsorbents are very expensive and their laborious production involves the use and waste of toxic materials and high energy.[8] To address these limitations, the development of new, cheaper, and more advanced adsorbents based on natural or waste materials, such as zeolites, clays, starch, fly ash, chitosan, etc., with sustainable and green production is recognized as a favorable approach.[5−7] Two natural minerals such as graphite, a source of graphene, and diatomaceous earth (DE) as a source of porous silica from diatoms, fossilized single-cell algae, are excellent choices with the potential to address these requirements.

Graphene, since its discovery in 2005, has attracted global attention because of its outstanding structural, thermal, mechanical, electrical, and adsorption properties.[9] These properties have been utilized for numerous applications, such as for the enhancement of composite materials, supercapacitors, batteries, and drug delivery.[9−12] Graphene has also been proven to be superior adsorbents for environmental applications in the removal of heavy metal ions and organic pollutants, showing high adsorption capacity and selectivity due to its ultrahigh surface area (≥1000 m^2/g) and tailorable functionalities.[10,11] In particular, graphene aerogels in the form of three-dimensional (3D) nanostructures combined with other materials (carbon nanotubes, nanoparticles, polymers) have attracted tremendous

Received: February 6, 2015
Accepted: April 2, 2015
Published: April 2, 2015

DOI: 10.1021/acsami.5b01159
ACS Appl. Mater. Interfaces 2015, 7, 11815−11823

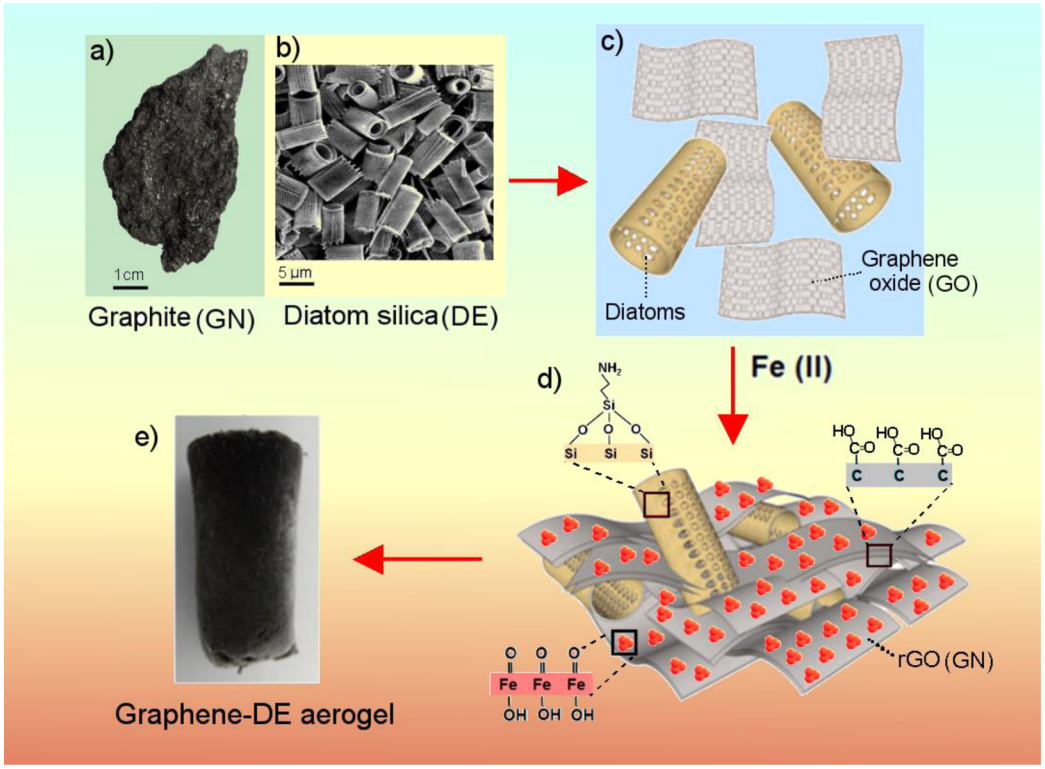

Figure 1. A schematic diagram for the synthesis of graphene-DE aerogels. (a) Graphite rock, (b) diatom silica microparticles from diatomaceous earth (DE), (c) the mixture of graphene oxide (GO) sheets and APTES modified diatoms prepared for (d) the graphene-DE hydrogel, and (e) the formation of the graphene-DE aerogel after the freeze-drying process. GO is reduced to graphene (rGO or GN) with the presence of some oxygen groups at the edges (defects) of the sheets.

attention for the design of advanced adsorbents based on their combined properties.[13,14]

Similarly, porous silica from DE has also been explored and practically demonstrated for many applications, such as water purification, beer and wine filtration, environmental remediation, optical sensing, and drug delivery, due to its excellent properties, which include high porosity, surface area (20−100 m^2/g), biocompatibility, chemical inertness, tailorable surface chemistry, and low cost ($300−500 per tonne).[15−21] DE is composed of fossilized diatoms with a unique 3D hierarchical and hollow structure with a specific pattern of nanopores build by amorphous silica.[15] In our previous work, we showed several concepts using surface functionalization by different silanes (3-aminopropyl-triethoxysilane (APTES), 3-mercaptopropyl-trimethoxysilane (MPTMS)) of porous DE microparticles to create very efficient adsorbents for the removal of heavy metals from polluted waters and the adsorption of gold and silver ions.[22,23] A number of other studies have also demonstrated the use of DE as an absorbent for the removal of specific heavy metal ions (e.g., Pb(II), Zn(II), Hg(II), Cd (II), and Cu(II)) from wastewater.[24−26] In our previous work, we also showed that, by modifying DE particles with graphene nanosheets, it is possible to combine these two materials and use them for pH selective drug delivery applications.[27]

In the present work, we propose a biomimetic approach based on two distinctive natural materials: porous silica from diatoms and graphene from graphite, which are combined and engineered into a self-assembled and functionalized 3D aerogel composite.[12,28] The concept is to synergize their exceptional adsorption properties, already proven for the removal of heavy metals and water contaminants. The preparation of the proposed graphene-DE aerogels is graphically presented in Figure 1. The enhanced adsorption of mercury (Hg) is proposed due to the combination of several factors, including the large 3D network surface area of the graphene nanosheets and diatom particles where the Hg ions can be physically trapped, and the presence of amino (at the modified diatom surface) and oxygen functional groups (on the edge of the graphene nanosheets), and iron oxide nanoparticles with their strong affinity for Hg ions.[29−31] The structural characteristics of the prepared aerogel composites, their adsorption capacity, and influence of pH on adsorption performance and kinetics for Hg ions were evaluated. Finally, the prepared adsorbents for the removal of Hg from contaminated waters were explored to demonstrate their application for real water purification.

2. EXPERIMENTAL SECTION

2.1. Materials and Chemicals. Natural graphite rocks (Uley, Eyre Peninsula, South Australia, Australia) is supplied from a local mining site and milled into a fine powder using a benchtop ring mill (Rocklabs). DE rocks were obtained from a diatomite mining company (Mount Sylvia Pty. Ltd., Queensland, Australia). Diatom samples in the form of ultrapure silica microcapsules (frustules) were prepared from the raw DE material using several purification steps, as described in our previous work.[18,21] Iron sulfate ($FeSO_4·7H_2O$, Sigma-Aldrich), 3-aminopropyl-trimethoxysilane (APTES, Sigma-Aldrich), potassium permanganate ($KMnO_4$, Sigma-Aldrich), mecury chloride-(II) ($HgCl_2$, Sigma-Aldrich), 99.7% isopropanol (Chem-Supply), 98% sulfuric acid (H_2SO_4, Chem-Supply), phosphoric acid (H_3PO_4, Chem-Supply), 30% hydrogen peroxide (H_2O_2, Chem-Supply), 35% hydrochloric acid (HCl, Chem-Supply), 69% nitric acid (HNO_3, Chem-Supply), sodium hydroxide (NaOH, Chem-Supply), and ethanol (Chem-Supply) were used directly without further processing.

DOI: 10.1021/acsami.5b01159
ACS Appl. Mater. Interfaces 2015, 7, 11815−11823

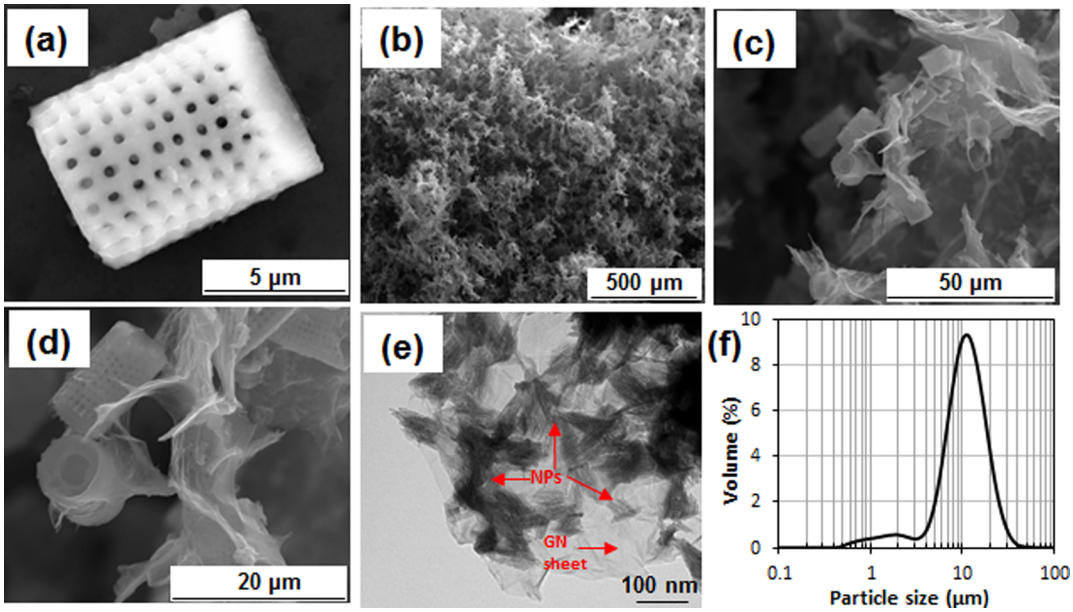

Figure 2. SEM images of (a) a single DE particle, (b) the prepared graphene-DE aerogel showing low-resolution image of the 3D network structure, and (c, d) high-resolution image of the graphene-DE aerogel. (e) TEM image of graphene (GN) sheets showing the presence of iron oxide nanoparticles (NPs). (f) The particle size distribution of DE particles dispersed in water.

High-purity milli-Q water (18.2 MΩ·cm at 25 °C, pH of 5.6) was used throughout the study, unless otherwise stated.

2.2. Surface Modification of Diatomaceous Earth (DE). Surface modification of the DE particles was performed by the typical silanization process.[23,27] The DE sample (1.0 g) was suspended in 30 mL of toluene under a static dry nitrogen atmosphere. Subsequently, 0.32 mL of water was added to the mixture that was stirred for 1−2 h at room temperature. Then, 1.7 mL of APTES was added dropwise into the mixture and refluxed for 6 h. The APTES modified DE (APTES-DE) were collected by centrifugation and washed several times with isopropanol and toluene before drying in a desiccator under vacuum at ambient temperature.

2.3. Preparation of Graphene Oxide (DE). Graphene oxide was prepared by the oxidation of natural graphite according to the improved Hummer's method.[32] Briefly, a 9:1 mixture of concentrated sulfuric acid and phosphoric acid (120:13 mL) was cooled to 4 °C. Upon stirring at room temperature, the cooled acid mixture was slowly added to the graphite powder (1 g) and potassium permanganate (6 g), then heated to 50 °C for about 12 h to form a thick paste. The finished reaction was cooled to room temperature and poured onto ice (150 mL) with 1 mL of hydrogen peroxide. The mixture was then washed with distilled water and 32% hydrochloric acid, followed by a repeated washing with ethanol. For each successive wash, the product was centrifuged at 4200 rpm for 2 h. The obtained GO was vacuum-dried overnight at room temperature.

2.4. Synthesis of Graphene-DE and Graphene Aerogels. GO (20 mg) was added into 10 mL of water and sonicated for 1 h to obtain a well-dispersed solution. Then, 5 mg of APTES-DE was added to the mixture, which was further sonicated for another 1 h to form a uniform graphene-DE dispersion. Different ratios of GO and DE were used to prepare the graphene-DE aerogels, but the most robust aerogel was prepared in the ratio of 4 to 1 for GO and DE, respectively. $FeSO_4{\cdot}7H_2O$ (1 mM) was then quickly added into the graphene-DE dispersion, and the solution was adjusted to acidic pH. The dispersion was poured into glass vials (25 mL) and sealed before placing into a 90 °C oil batch for 6−8 h. The obtained 3D black monoliths were first washed with water to remove any outside residues, then freeze-dried for 24 h to obtain the corresponding graphene-DE aerogels. Graphene aerogels were also prepared under the same condition as the graphene-DE aerogels except without the addition of DE.

2.5. Characterizations. The morphology of DE, GO, and graphene-DE aerogels were characterized by scanning electron microscopy (FE-SEM, Quanta 450, FEI, USA) and transmission eletron microscopy (FEI, Tecnai, G2 spirit TEM, USA) to confirm the 3D aerogel structure and decoration of the iron nanoparticles (NPs) on the graphene sheets. The size distribution of the DE particles in the water solution (1% w/v) was determined using the Mastersizer X (Malvern Instruments, U.K.). Fourier transform infrared (FTIR) spectroscopy (Nicolet 6700 Thermo Fisher) was used to identify the functional groups of GO and the reduction of GO to graphene by iron NPs recorded in the range of 500−4000 cm^{-1} in transmittance mode. The vibrational characteristics of GO and the graphene-DE aerogel were analyzed by Raman spectroscopy (LabRAM HR Evolution, Horiba Jvon Yvon Technology, Japan) using a 532 nm laser (mpc 3000) as the excitation source in the range of 500−3500 cm^{-1}. A 100× objective was used with a spot size of 100 μm. The laser power was kept at or below approximately 50%, and all spectra were collected using an intergration time of 10 s for 3 accumulations. The X-ray diffraction (600 Miniflex, Rigaco, Japan) measurement was performed to illuminate the composition of GO and the graphene-DE aerogel. Solution ICP-MS (7500cs, Alginate) was used to measure the final concentration of mercury(II) ions (Hg^{2+}) in the adsorption experiments. The specific surface area (SSA) of the prepared graphene-DE aerogel was determined using the methylene blue (MB) adsorption method by UV−vis spectroscopy (Shimadzu UV-1601, Japan). Details are provided in the Supporting Information.

2.6. Batch Adsorption of Mercury Ions. The adsorption capacity of the graphene-DE aerogels was determined using a series of known concentration of Hg^{2+} ions (from 50 to 400 mg/L) in water (pH 6.5) by placing the graphene-DE aerogels (10 mg) in 250 mL of the Hg solution at ambient temperature (25 ± 1 °C). The adsorbent−solution mixture was stirred for 90 min; then, samples were taken every 5 min and measured with ICP-MS to determine the Hg concentration after centrifugation to separate the supernantant.

For testing the effect of pH in the range of pH 2−10 on the removal of Hg, the pH of the Hg solution (200 mg/L) was adjusted to the targeted value by adding HCl or NaOH and was kept constant during the experiment. Kinetic experiments were performed at pH 6.5. For each adsorption test performed, the supernatant was removed and immediately filtered through a cellulose acetate membrane with a pore size of 0.22 μm, and the Hg concentration was determined via ICP-MS. Prior to the analysis, the samples were acidified with 2% HNO_3. The amount of heavy metal ions Q_t (mg/g) adsorbed with the graphene-DE aerogel at time t, was calculated using the following eq 1

DOI: 10.1021/acsami.5b01159
ACS Appl. Mater. Interfaces 2015, 7, 11815−11823

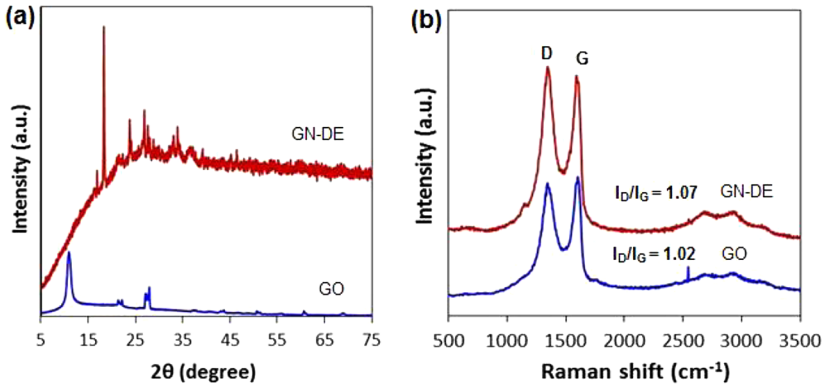

Figure 3. (a) XRD patterns and (b) Raman spectra of the GO and graphene-DE (GN-DE) aerogel.

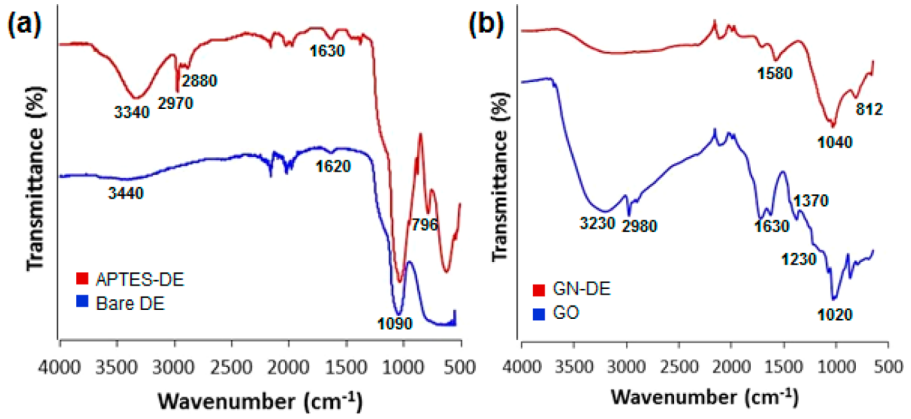

Figure 4. FTIR plots of (a) bare diatom (DE) and APTES modified DE (APTES-DE), and (b) graphene oxide (GO) and graphene-DE (GN-DE) aerogel.

$$Q_t = \frac{(C_0 - C_t)*V}{M} \quad (1)$$

where C_0 and C_t are the initial and time t concentrations of the heavy metal ions solution (mg/L), respectively. V is the volume of solution (L), and M is the mass of the aerogel used (g).

Finally, to simulate practical applications, comparative adsorption studies for three different sources of water, milli-Q, tap, and river water (Torrens River, Adelaide, Australia) were spiked with Hg^{2+} to provide the desired Hg concentration (100 mg/L) using 10 mg of adsorbent. The model system (milli-Q water solution) was adjusted to pH 6.5, whereas the natural water samples (tap and river water) were used as is (natural pH of solution already ~6−7). The adsorbent−solution mixture was stirred for 90 min; then, a sample was taken and the Hg concentration remaining in the mixture was measured. An average of three measurements was taken for all experiments.

3. RESULTS AND DISCUSSION

3.1. Structural and Chemical Characterization of Graphene-DE Aerogels. A SEM image showing the structure of the diatom particles prepared from the raw DE material (rocks) is presented in Figure 2a. The image depicts a characteristic structure of *Aulacoseira* sp. (major diatom species, >90%), with a perforated cylindrical shell and an opening at one end. Regularly spaced rows of pores of ~300−500 nm in diameter are located along the frustule shell wall. The size of the DE particles was measured by dynamic light scattering, and a monodispersed distribution curve with the maximum peak at 15 μm (Figure 2f) was obtained, confirming the presence of single DE frustules, eliminating the possibilities of aggregates and fractures.

The prepared graphene-DE aerogels after freeze-drying show a black and spongy appearance, as presented in Figure 1e. The cylindrical shape of the aerogel is a result of the glass mold used during the preparation. Other sizes and shapes of the aerogel can also be prepared if required. In Figure 2b, the aerogel structure reveals a characteristic 3D network composed of graphene and DE particles. Higher resolution of SEM images (Figure 2c,d) illustrates in more detail the interconnected porous structure. The pore walls consist of very thin layers of stacked graphene sheets with DE particles trapped in between, hence avoiding the agglomeration between them. Although all the aerogel imaged under SEM showed that their surface is decorated by DE particles, the coverage was not homogeneous. As can be seen from the low-magnification TEM image (Figure 2e), the graphene sheets (without DE) have a large number of iron oxide (αFeOOH) nanoparticles (NPs) decorated on them.

The calculated specific surface area of the prepared graphene-DE aerogel (368.0 ± 2 m^2/g) is higher compared to that of the graphene aerogel without DE (208.9 ± 2 m^2/g). The higher porosity and larger surface area of the graphene-DE aerogels compared to those of graphene aerogels without DE are due to the presence of the DE particles acting as spacers in the graphene sheets. Simultaneously, the reduced GO sheets and DE anchored with the αFeOOH nanoparticles that self-assembled into the hydrogel is driven by the combined hydrophobic and $\pi-\pi$ stacking interactions, due to the decrease of oxygenated groups on the GO surface. Thus, the functional groups on the surface of GO also play an important role in the aerogel preparation.

DOI: 10.1021/acsami.5b01159
ACS Appl. Mater. Interfaces 2015, 7, 11815−11823

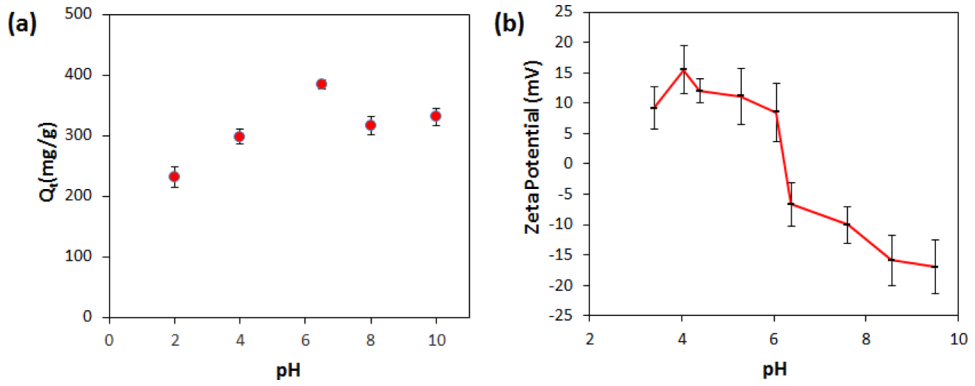

Figure 5. (a) Adsorption capacity and (b) zeta potential of graphene-DE aerogel measured in the range of pH 2−10. Condition: Hg concentration = 200 mg/L.

Figure 3a shows the X-ray diffraction (XRD) patterns of GO and the graphene-DE aerogel. The intensive peak at $2\theta = 10.8°$ (d-spacing = 0.86 nm) represents the (001) reflection of GO due to the presence of oxygen-containing groups during the oxidation of graphite. In contrast, the disappearance of the peak at 10.8−18.3° for the graphene-DE aerogel provides further evidence of the GO reduction.[33] For the graphene-DE aerogels, the major diffraction peak is assigned to the orthorhombic structure of the α-FeOOH (JCPDS card No. 29-0713), and the broad peaks around 15° and 35° present the existence of the amorphous silica ($-SiO_2$) on the DE surface.[34,35]

Raman analysis of the graphene-DE aerogel prepared by the synthesis route shown in Figure 3b provides further evidence for the attachment of DE and graphene. The spectra of GO and graphene-DE aerogel both display the two characteristic peaks (i.e., G and D band). The G band corresponds to the in-plane vibration of sp^2 to sp^3 hybridized carbon originating from the destruction of the sp^2 structures of the graphite or due to the covalent attachment of functional groups. The D band is associated with the disorder in the graphitic structure.[28] The G band of the graphene-DE aerogel (1594 cm^{-1}) was slightly shifted compared to that of pure GO (1591 cm^{-1}), revealing the charge transfer between the graphene sheets, DE, and α-FeOOH nanoparticles.[34] The intensity ratio of the D and G bands (I_D/I_G) in the graphene-DE aerogel (1.07) also enhanced after the reduction compared with that of GO (1.02), representing the improvement of the disordered graphene sheets.

FTIR results of the modified DE further confirm the presence of the organic moieties on the DE surface, compared to bare DE used as the control, and are presented in Figure 4a. The characteristic peak of the diatomite silica framework at wavenumber 1090 cm^{-1} was observed, which can be attributed to the stretching modes of Si−O−Si and Si−O−C, while the Al−O−Si stretching vibration is indicated at 796 cm^{-1}. The hydroxyl (−OH) peaks at 3340 and 1630 cm^{-1} present the stretching vibrations of adsorbed water and zeolitic water sourced from the DE, respectively. The DE sample modified with APTES gave rise to a spectrum similar to that of the reference. However, an additional band for the $-CH_2-$ asymmetric stretching mode was observed at 2970 cm^{-1} and the C−H symmetric stretching mode appeared at 2880 cm^{-1} for APTES-DE, which is directly related to the carbon chain of organosilane molecules,[18,22,27,36] therefore, confirming the successful modification of the diatom surface by APTES.

Furthermore, the FTIR spectra of GO presents the following absorbance bands, O−H stretching vibrations at 3230 cm^{-1}, C═C from unoxidized sp^2 C−C bonds at 1630 cm^{-1}, C−O vibrational at 1230 cm^{-1}, C═O stretching of the COOH at 1730 cm^{-1}, HC═C− at 2980 cm^{-1}, and CO−H at 1370 cm^{-1} (Figure 4b).[32] The absorbance bands of the carbonyl and epoxy groups are not present in the graphene-DE aerogel, indicating the effective reduction of the graphene sheets. The adsorption bands at 1580, 1040, and 812 cm^{-1} in the graphene-DE aerogel are the characteristic peaks of Fe containing Fe−OH and Fe−O groups, respectively.[37,38] These results conclude that the hydrogels were formed by the coassembly of graphene sheets, DE, and αFeOOH nanoparticles as shown from the above characterizations.

3.2. Effect of pH. The effect of pH on the Hg^{2+} ions removal was examined for the graphene-DE aerogel and is presented in Figure 5a. The graph presents the change in adsorption capacity of the graphene-DE aerogel on Hg^{2+} ions in the pH range of 2−10. The result indicates that, during the adsorption process, the solution pH has an influence on the adsorption of Hg by the graphene-DE aerogel. The adsorption capacities increased from pH 2 to 6.5 and then slightly decreased with pH above 6.5. We propose two major mechanisms for the capturing of Hg ions by the aerogel, which is physical trapping and binding with available amino and oxygen groups on the graphene-DE aerogel. To better understand this process and the influence of pH on the adsorption capacity, the zeta potential of the graphene-DE aerogel is explored and presented in Figure 5b.

The zeta potential of the graphene-DE aerogel in different pHs shows that the prepared aerogel is positively charged (+10 mV) below pH 6, which repulses the Hg^{2+} cations, resulting in the low mercury uptake compared to pH 6 and above. With increasing pH > 6, the graphene-DE aerogel surface becomes more negative (> −10 mV), which increases the attraction of Hg ions and their adsorption. The surface charge of the graphene-DE aerogels depends on the surface charge of both the graphene sheets and the αFeOOH nanoparticles anchored on its surface. Several reports have shown that graphene is negatively charged in the pH range of 2−14, while the oxyhydroxide surface becomes positive at pH lower than 6 and slightly negative at pH higher than 6.[39−41] Although the surface charge of the aerogel becomes more negative at higher pH, the mercury uptake slightly decreases. Such behavior is likely attributed to the formation of $Hg(OH)^{3-}$ due to the increase in concentration of OH^-,[41,42] which are repulsed by the negatively

DOI: 10.1021/acsami.5b01159
ACS Appl. Mater. Interfaces 2015, 7, 11815−11823

charged graphene-DE aerogel surface, consequently lowering the Hg adsorption. This observation is in agreement with previous studies showing that the Hg adsorption has been monotonically decreased on an activated carbon surface by increasing pH, due to the competitive adsorption between the mercury ions and increased OH^-, resulting in the active sites being occupied by OH^- on the adsorbent.[4] In addition, the mercury's speciation at different pHs could also play a role, especially at higher pH, where some Hg^{2+} ions can be blocked in the presence of high concentrations of chloride ions by association with OH (HgClOH) and, therefore, reducing their adsorption.[3]

3.3. Adsorption Kinetics. The adsorption performance of the prepared graphene-DE compared with that of the graphene aerogel for adsorption of Hg^{2+} ions is summarized in Figure 6.

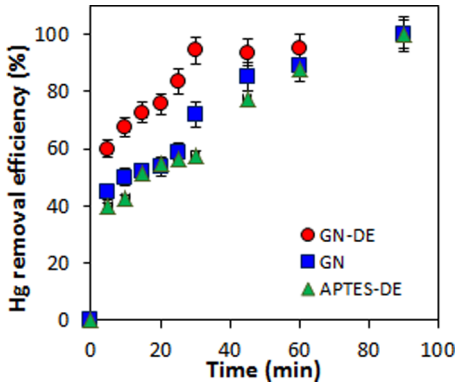

Figure 6. Time dependence of Hg^{2+} adsorption on the graphene-DE (GN-DE) aerogel, graphene (GN) aerogel (with αFeOOH nanoparticles), and APTES modified diatom (APTES-DE). Conditions: Hg concentration = 200 mg/L; pH = 6.5.

The graph shows that the rate of Hg^{2+} uptake was initially high for the graphene-DE aerogels with about 60% removed during the first 5 min. There was a gradual reduction in the rate of removal afterward, but about 90% of Hg^{2+} ions were removed within 30 min before reaching equilibrium. The fast kinetics and ability to remove Hg ions is attributed to the combination of three factors, (1) the electrostatic attraction between the oxides (αFeOOH nanoparticles and graphene edges) and Hg ions, (2) the ion exchange in the aqueous solution, and (3) the amino functional groups present on the APTES modified DE.[23,28] To confirm this conclusion, the influence of the graphene-αFeOOH and APTES-DE for Hg adsorption is explored by control experiments to determine separately the adsorption efficiency for both components (Figure 6). The results show that both substrates have considerable adsorption capacity for Hg, which confirms that both proposed adsorption mechanisms is via interaction with oxygen and amino functional groups. Interestingly, the adsorption performance of the graphene-DE aerogel is lower than the combined performance of the graphene-αFeOOH and APTES-DE from the individual experiments. This can be explained by the blocking of some active sites (O and NH_2) in the interconnected 3D network structure of the graphene-DE aerogel and also by the lowering of its surface area.

The adsorption kinetics of the graphene-DE aerogel compared to that of the graphene aerogel control was analyzed using the Lagergren pseudo-first-order and pseudo-second-order kinetic models. Pseudo-first-order rate expression of the Lagergen equation[43] is given as

$$\log(Q_e - Q_t) = \log Q_e - k_1 t \quad (2)$$

where Q_e and Q_t are the amount of mercury adsorbed in mg/g at equilibrium and at time t (min), respectively, and k_1 1/min is the rate constant of the pseudo-first-order adsorption. The adsorption rate constant can be determined from the slope of the linear plot of $\log(Q_e - Q_t)$ versus t.

Pseudo-second-order rate expression[41] is given as

$$\frac{t}{Q_t} = \frac{1}{Q_e^2 k_2} + \frac{t}{Q_e} \quad (3)$$

where k_2 (g/mg min) is the pseudo-second-order rate constant. k_2 can be calculated from the slope and intercept of the plot t/Q_t versus t.

The kinetics data obtained from the linearized plots for pseudo-first- and pseudo-second-order kinetic models are presented in Table 1. The linear correlation coefficient R^2 values for the pseudo-first-order kinetic model were 0.85 and 0.94, for the graphene-DE and graphene aerogels, respectively (Figure S1, Supporting Information). However, greater linear fits with a correlation of 0.98 were achieved for both types of aerogels when the pseudo-second-order kinetic model was applied. This suggests that the adsorption data for the kinetics studies are well-represented by the pseudo-second-order kinetic model.

Table 1. Lagergren Pseudo-First-Order and Pseudo-Second-Order Kinetics Parameters of Hg^{2+} Adsorption onto Graphene-DE and Graphene Aerogels, and APTES-DE

	pseudo-first-order		pseudo-second-order	
adsorbent	R^2	k_1 (1/min)	R^2 (g/mg min)	k_2 ($\times 10^{-3}$)
graphene-DE	0.848	0.048	0.981	3.90
graphene	0.938	0.034	0.980	1.82
APTES-DE	0.941	0.030	0.979	2.40

The pseudo-second-order has been widely used to explain the removal of different contaminants from the water, which assumes a chemisorption process involving covalent forces and ion exchange.[41,44] The corresponding rate constants (k_2) for the graphene-DE and graphene aerogels calculated from the slopes of the plots are 3.90×10^{-3} and 1.82×10^{-3} g/mg min, respectively. The reactivity of the graphene-DE aerogel is 2 times higher than that of the graphene aerogel; hence, the graphene-DE aerogel achieved a greater mercury adsorption capacity.

3.4. Adsorption Isotherm. At an initial mercury concentration of ~400 mg/L, an adsorption capacity of 528 mg/g was obtained for the graphene-DE aerogel, which can be described as outstanding compared with other adsorbents. The plot of equilibrium concentration versus adsorption capacity (Figure 7) indicated that the adsorption process was a function of the initial concentration. However, this concentration-dependent adsorption is applicable only to a certain extent, as the adsorption becomes a concentration-independent process as soon as it reaches the maximum adsorption capacity. It is obvious that, for the range of the examined Hg concentrations, the adsorption saturation occurs.

DOI: 10.1021/acsami.5b01159
ACS Appl. Mater. Interfaces 2015, 7, 11815−11823

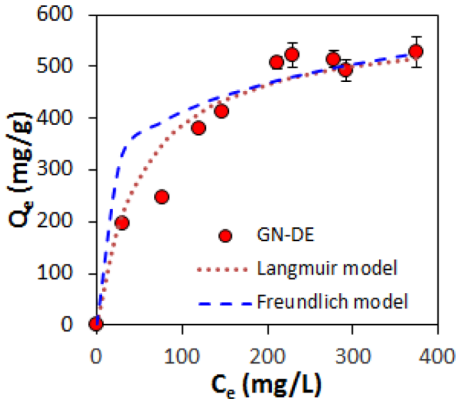

Figure 7. Adsorption performance of graphene-DE (GN-DE) aerogel at different Hg concentrations fitted with equilibrium models. Condition: pH = 6.5.

To analyze the adsorption behavior of the graphene-DE aerogel, the data in Figure 7 were plotted using the sorption Freundlich and Langmuir isotherm models.[22,45]

The Langmuir isotherm is expressed as follows (4)

$$Q_e = \frac{1}{Q_{max} b} + \frac{C_{eq}}{q_{max}} \quad (4)$$

where Q_e is the adsorption capacity (mg/g), C_{eq} is the Hg^{2+} concentration (mg/L) at equilibrium, and b and Q_{max} are the Langmuir constant (l/mg) determined by the intercept and slope of the linear plot of Q_e versus C_{eq}, respectively.

The Freundlich isotherm is presented by eq 5

$$\log Q_e = \log K_f + \frac{1}{n} \log C_{eq} \quad (5)$$

where K_f represents the Freundlich adsorption constant (l/mg) and $1/n$ is the adsorption intensity. These parameters can be calculated from the intercept and slope of the plot log Q_e versus log C_{eq}, respectively.

Correlation coefficients of R^2 = 0.87 and 0.95 were achieved for the Freundlich and Langmuir models, respectively (Figure S2 and Table S1, Supporting Information). This result indicates that the adsorption fits well with the Langmuir model, suggesting monolayer coverage sorption of Hg^{2+} ions on the surface of the graphene-DE aerogels. The calculated maximum adsorption capacity for Hg^{2+} removal by the graphene-DE aerogels in this work was found to be higher than that by carbon aerogels (35 mg/g),[46] APTES-activated carbon (121 mg/g),[47] thiol functionalized magnetic mesoporous silica,[48] and our previous work with 3-mercaptopropyl-trimethoxysilane-DE (MPTMS-DE) material (185.5 mg/g).[23] However, most of the adsorption results for metal ions removal in the literature were recorded at optimal pH values, which had a significant effect on the adsorption capacities of the adsorbent. Furthermore, the SEM images of our graphene-DE aerogels after Hg adsorption showed that their 3D structure is preserved during the adsorption process (Figure S3, Supporting Information).

3.5. Removal of Mercury from Different Water Sources. In a practical application for the removal of mercury by the graphene-DE aerogel (10 mg dosage), adsorption experiments were conducted on natural water samples (tap and river water) that were spiked with 100 mg/L of Hg^{2+} solution compared with milli-Q water as the model system and are presented in Figure 8. The maximum adsorption capacity of the graphene-DE aerogel achieved was 362, 308, and 336 mg/g (±0.5 mg/g) in milli-Q, river, and tap water, respectively.

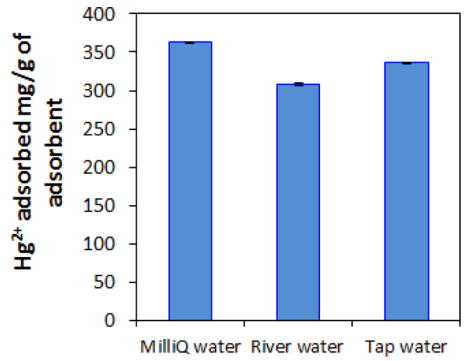

Figure 8. Batch tests of graphene-DE aerogel for Hg^{2+} ions removal in different water sources. Conditions: Hg concentration = 100 mg/L, pH ~ 6–7.

The results show that the Hg concentration remaining in the river water is slightly higher compared to that in milli-Q water. This might be attributed to the complicated matrixes of the river water, which contains various inorganic and organic substances. These ions are in competition with Hg^{2+} adsorption, and the saturation of binding sites of the adsorbent justifies the difference in mercury uptake for the different water sources. However, there is no major interference for the removal efficiency of the graphene-DE aerogels in the different waters. The slightly higher efficiency obtained for tap water compared to that for river water is likely due to the higher concentrations of competitive ions in the river water, as explained earlier.

4. CONCLUSIONS

We demonstrated for the first time the synthesis of a self-assembled aerogel composed of graphene sheets and DE particles decorated with αFeOOH nanoparticles within a robust and interconnected 3D network. The prepared aerogel is an effective adsorbent for mercury removal from high concentration levels, which showed an outstanding adsorption performance with an adsorption capacity of >500 mg/g (at 400 mg/L Hg^{2+}) of Hg ions, exceeding many competing adsorbents. This new adsorbent prepared by a simple process from two low cost natural materials widely available from the mining industry (graphite and DE) and based on its excellent adsorption performance is a promising solution for the development of efficient and cost-competitive adsorbents. The adsorbents can be prepared into different structural shapes (depending on the reaction vessel) and utilized in different forms (flat, circular, cube, etc.) for different scenarios for the removal of mercury and other toxic contaminants from the water (industrial, environmental, and drinking).

■ ASSOCIATED CONTENT

Supporting Information

The information for measuring the specific surface area of the aerogel with the methylene blue adsorption method; figures and tables showing the pseudo-first- and pseudo-second-order kinetics, and Langmuir and Freundlich plots for the adsorption of Hg; low- and high-resolution SEM images and EDAX of graphene-DE aerogels after mercury adsorption, respectively.

DOI: 10.1021/acsami.5b01159
ACS Appl. Mater. Interfaces 2015, 7, 11815–11823

This material is available free of charge via the Internet at http://pubs.acs.org.

AUTHOR INFORMATION

Corresponding Author

*E-mail: dusan.losic@adelaide.edu.au (D.L.).

Author Contributions

The manuscript was written through contributions of all authors. All authors have given approval to the final version of the manuscript.

Notes

The authors declare no competing financial interest.

ACKNOWLEDGMENTS

This work was supported by The Australian Research Council (FT110100711), The University of Adelaide, School of Chemical Engineering, Valence Industries Ltd., and Archer Exploration Ltd. The authors also thank Mount Sylvia Diatomite Pty. Ltd. for providing the DE materials and to Ms. Aoife McFadden (Adelaide Microscopy) for her technical support for ICP-MS measurement.

REFERENCES

(1) Boening, D. W. Ecological effects, transport, and fate of mercury: A general review. *Chemosphere* **2000**, *40*, 1335−1351.
(2) Bose-O'Reilly, S.; McCarty, K. M.; Steckling, N.; Lettmeier, B. Mercury exposure and children's health. *Curr. Probl. Pediatr. Adolesc. Health Care* **2010**, *40*, 186−215.
(3) Lu, X.; Huangfu, X.; Ma, J. Removal of trace mercury(II) from aqueous solution by in situ formed Mn−Fe (hydr)oxides. *J. Hazard. Mater.* **2014**, *280*, 71−78.
(4) *World Health Organization Guidelines for Drinking-water Quality*, 3rd ed.; Incorporating The First and Second Addenda, Vol 1; WHO Press: Geneva, 2008; pp 1−668. http://www.who.int/water_sanitation_health/dwq/fulltext.pdf (accessed Dec 1, 2014).
(5) Theron, J.; Walker, J. A.; Cloete, T. E. Nanotechnology and water treatment: Applications and emerging opportunities. *Crit. Rev. Microbiol.* **2008**, *34*, 43−69.
(6) Li, G.; Zhao, Z.; Liu, J.; Jiang, G. Effective heavy metal removal from aqueous systems by thiol functionalized magnetic mesoporous silica. *J. Hazard. Mater.* **2011**, *192*, 277−283.
(7) Walcarius, A.; Mercier, L. Mesoporous organosilica adsorbents: Nanoengineered materials for removal of organic and inorganic pollutants. *J. Mater. Chem.* **2010**, *20*, 4478−4511.
(8) Zhao, G.; Li, J.; Ren, X.; Chen, C.; Wang, X. Few-layered graphene oxide nanosheets as superior sorbents for heavy metal ion pollution management. *Environ. Sci. Technol.* **2011**, *45*, 10454−10462.
(9) Schedin, F.; Geim, A. K.; Morozov, S. V.; Hill, E. W.; Blake, P.; Katsnelson, M. I.; Novoselov, K. S. Detection of individual gas molecules adsorbed on graphene. *Nat. Mater.* **2007**, *6*, 652−655.
(10) Bai, H.; Li, C.; Shi, G. Functional composite materials based on chemically converted graphene. *Adv. Mater.* **2011**, *23*, 1089−1115.
(11) Stoller, M. D.; Park, S.; Zhu, Y.; An, J.; Ruoff, R. S. Graphene-based ultracapacitors. *Nano Lett.* **2008**, *8*, 3498−3502.
(12) Sui, Z.; Meng, Q.; Zhang, X.; Ma, R.; Cao, B. Green synthesis of carbon nanotube-graphene hybrid and their use as versatile agents for water purification. *J. Mater. Chem.* **2012**, *22*, 8767−8771.
(13) Kemp, K. C.; Seema, H.; Saleh, M.; Le, N. H.; Mahesh, K.; Chandra, V.; Kim, K. S. Environmental applications using graphene composites: Water remediation and gas adsorption. *Nanoscale* **2013**, *5*, 3149−3171.
(14) Lin, Y.; Ehlert, G. J.; Bukowsky, C.; Sodano, H. A. Superhydrophobic functionalized graphene aerogels. *ACS Appl. Mater. Interfaces* **2011**, *3*, 2200−2203.
(15) Losic, D.; Mitchell, J. G.; Voelcker, N. H. Diatomaceous lessons in nanotechnology and advanced materials. *Adv. Mater.* **2009**, *21*, 2947−2958.
(16) Gordon, R.; Losic, D.; Tiffany, M. A.; Nagy, S. S.; Sterrenburg, F. A. S. The glass menagerie: Diatoms for novel applications in nanotechnology. *Trends Biotechnol.* **2009**, *27*, 116−127.
(17) Lopez, P. J.; Desclés, J.; Allen, A. E.; Bowler, C. Prospects in diatom research. *Curr. Opin. Biotechnol.* **2005**, *16*, 180−186.
(18) Aw, M. S.; Simovic, S.; Addai-Mensah, J.; Losic, D. Silica microcapsules from diatoms as new carrier for delivery of therapeutics. *Nanomedicine* **2011**, *6*, 1159−1173.
(19) Aw, M. S.; Simovic, S.; Yu, Y.; Addai-Mensah, J.; Losic, D. Porous silica microshells from diatoms as biocarrier for drug delivery applications. *Powder Technol.* **2012**, *223*, 52−58.
(20) Yu, Y.; Addai-Mensah, J.; Losic, D. Synthesis of self-supporting gold microstructures with three-dimensional morphologies by direct replication of diatom templates. *Langmuir* **2010**, *26*, 14068−14072.
(21) Kabiri, S.; Kurkuri, M. D.; Kumeria, T.; Losic, D. Frit-free PDMS microfluidic device for chromatographic separation and on-chip detection. *RSC Adv.* **2014**, *4*, 15276−15280.
(22) Yu, Y.; Addai-Mensah, J.; Losic, D. Chemical functionalization of diatom silica microparticles for adsorption of gold (III) ions. *J. Nanosci. Nanotechnol.* **2011**, *11*, 10349−10356.
(23) Yu, Y.; Addai-Mensah, J.; Losic, D. Functionalized diatom silica microparticles for removal of mercury ions. *Sci. Technol. Adv. Mater.* **2012**, *13*, 015008−015018.
(24) Merrifield, J. D.; Davids, W. G.; MacRae, J. D.; Amirbahman, A. Uptake of mercury by thiol-grafted chitosan gel beads. *Water Res.* **2004**, *38*, 3132−3138.
(25) Ma, X.; Li, Y.; Ye, Z.; Yang, L.; Zhou, L.; Wang, L. Novel chelating resin with cyanoguanidine group: useful recyclable materials for Hg(II) removal in aqueous environment. *J. Hazard. Mater.* **2011**, *185*, 1348−1354.
(26) Zhang, X. Y.; Wang, Q. C.; Zhang, S. Q.; Sun, X. J.; Zhang, Z. S. Stabilization/solidification (S/S) of mercury-contaminated hazardous wastes using thiol-functionalized zeolite and portland cement. *J. Hazard. Mater.* **2009**, *168*, 1575−1580.
(27) Kumeria, T.; Bariana, M.; Altalhi, T.; Kurkuri, M.; Gibson, C. T.; Yang, W.; Losic, D. Graphene oxide decorated diatom silica particles as new nano-hybrids: Towards smart natural drug microcarriers. *J. Mater. Chem. B* **2103**, *1*, 6302−6311.
(28) Cong, H.-P.; Ren, X.-C.; Wang, P.; Yu, S.-H. Macroscopic multifunctional graphene-based hydrogels and aerogels by a metal ion induced self-assembly process. *ACS Nano* **2012**, *6*, 2693−2703.
(29) Barrow, N. J.; Cox, V. C. The effects of pH and chloride concentration on mercury sorption. I. By goethite. *J. Soil Sci.* **1992**, *43*, 295−304.
(30) Kim, C. S.; Rytuba, J. J.; Brown, G. E., Jr. EXAFS study of mercury(II) sorption to Fe- and Al-(hydr)oxides: I. Effects of pH. *J. Colloid Interface Sci.* **2004**, *271*, 1−15.
(31) Bäckström, M.; Dario, M.; Karlsson, S.; Allard, B. Effects of a fulvic acid on the adsorption of mercury and cadmium on goethite. *Sci. Total Environ.* **2003**, *304*, 257−268.
(32) Marcano, D. C.; Kosynkin, D. V.; Berlin, J. M.; Sinitskii, A.; Sun, Z.; Slesarev, A.; Alemany, L. B.; Lu, W.; Tour, J. M. Improved synthesis of graphene oxide. *ACS Nano* **2010**, *4*, 4806−4814.
(33) Shin, H.-J.; Kim, K. K.; Benayad, A.; Yoon, S.-M.; Park, H. K.; Jung, I.-S.; Jin, M. H.; Jeong, H.-K.; Kim, J. M.; Choi, J.-Y.; Lee, Y. H. Efficient reduction of graphite oxide by sodium borohydride and its effect on electrical conductance. *Adv. Funct. Mater.* **2009**, *19*, 1987−1992.
(34) Ho, Y. S. Citation review of lagergren kinetic rate equation on adsorption reactions. *Scientometrics* **2004**, *59*, 171−177.
(35) Ho, Y. S.; Ng, J. C. Y.; McKay, G. Kinetics of pollutant sorption by biosorbents: review. *Sep. Purif. Methods* **2000**, *29*, 189−232.
(36) Song, N.-N.; Yang, H.-T.; Liu, H.-L.; Ren, X.; Ding, H.-F.; Zhang, X.-Q.; Cheng, Z.-H. Exceeding natural resonance frequency limit of monodisperse Fe_3O_4 nanoparticles via superparamagnetic relaxation. *Sci. Rep.* **2013**, *3*, 3161−3165.

DOI: 10.1021/acsami.5b01159
ACS Appl. Mater. Interfaces 2015, 7, 11815−11823

(37) Mi, Y.; Wang, Z.; Liu, X.; Yang, S.; Wang, H.; Ou, J.; Li, Z.; Wang, J. A simple and feasible in-situ reduction route for preparation of graphene lubricant films applied to a variety of substrates. *J. Mater. Chem.* **2012**, *22*, 8036−8042.
(38) Bariana, M.; Aw, M. S.; Kurkuri, M.; Losic, D. Tuning drug loading and release properties of diatom silica microparticles by surface modifications. *Int. J. Pharm.* **2013**, *443*, 230−241.
(39) Shou, Q.; Cheng, J.; Zhang, L.; Nelson, B. J.; Zhang, X. Synthesis and characterization of a nanocomposite of goethite nanorods and reduced graphene oxide for electrochemical capacitors. *J. Solid State Chem.* **2012**, *185*, 191−197.
(40) Ou, P.; Xu, G.; Ren, Z.; Hou, X.; Han, G. Hydrothermal synthesis and characterization of uniform α-FeOOH nanowires in high yield. *Mater. Lett.* **2008**, *62*, 914−917.
(41) Tran, D. N. H.; Kabiri, S.; Losic, D. A green approach for the reduction of graphene oxide nanosheets using non-aromatic amino acids. *Carbon* **2014**, *76*, 193−202.
(42) Li, D.; Muller, M. B.; Gilje, S.; Kaner, R. B.; Wallace, G. G. Processable aqueous dispersions of graphene nanosheets. *Nat. Nanotechnol.* **2008**, *3*, 101−105.
(43) Kokkinos, E.; Simeonidis, K.; Zouboulis, A.; Mitrakas, M. Mercury removal from drinking water by single iron and binary iron-manganese oxyhydroxides. *Desalin. Water Treat.* **2014**, 1−9.
(44) Ho, Y.-S. Review of second-order models for adsorption systems. *J. Hazard. Mater.* **2006**, *136*, 681−689.
(45) Chen, Z.; Ma, W.; Han, M. Biosorption of nickel and copper onto treated alga (*Undaria pinnatifida*): Application of isotherm and kinetic models. *J. Hazard. Mater.* **2008**, *155*, 327−333.
(46) Goel, J.; Kadirvelu, K.; Rajagopal, C.; Garg, V. K. Removal of mercury (II) from aqueous solution by adsorption on carbon aerogel: Response surface methological approach. *Carbon* **2005**, *43*, 197−200.
(47) Zhu, J.; Yang, J.; Deng, B. Enhanced mercury ion adsorption by amine-modified activated carbon. *J. Hazard. Mater.* **2008**, *166*, 866−872.
(48) Hakami, O.; Zhang, Y.; Banks, C. J. Thiol-functionalised mesoporous silica-coated magnetite nanoparticles for high efficiency removal and recovery of Hg from water. *Water Res.* **2012**, *46*, 3913−3922.

DOI: 10.1021/acsami.5b01159
ACS Appl. Mater. Interfaces 2015, 7, 11815−11823